emerald PUBLISHING

International Journal of Numerical Methods for Heat and Fluid Flow

Suprachoroidal shunts for treatment of glaucoma: a comparison based on numerical simulations

Journal:	*International Journal of Numerical Methods for Heat and Fluid Flow*
Manuscript ID	HFF-12-2016-0508.R1
Manuscript Type:	Research Article
Keywords:	Numerical modelling, Finite element method, Eye, Ocular Pathology, Patient specific, Surgery

Suprachoroidal shunts for treatment of glaucoma: a comparison based on numerical simulations

ABSTRACT

Purpose: The purpose of this paper is to compare the fluid dynamic performance of two Aqueous Humor (AH) ocular drainage devices, the SOLX® Gold Micro Shunt (GMS) and the novel Silicon Shunt Device (SSD), implanted by surgeons in human eyes to reduce the IntraOcular Pressure (IOP) towards physiological values, by draining the AH from the Anterior Chamber (AC) to the Suprachoroidal Space (SCS), in order to cure eyes with glaucoma.

Design/methodology/approach: The generalised porous medium model is solved to simulate the AH flow through the two ocular drainage devices and the surrounding porous tissues of the eye.

Findings: In the GMS, probable stagnation regions have been found, due to very small AH velocity values inside the device and to the surrounding tissues, creating possible blockage and malfunction of the device. The simple microtubular geometry of the novel SSD allows to have a regular AH flow and to choose shunts with different diameters and/or with the presence of radial holes, based on patient needs, with consequent reduction of post-operative complications.

Research limitations/implications: The present model will be further developed taking into account the insertion of the present drainage devices inside the anterior section of the eye. The present results show the comparative fluid dynamic performance of the two shunts considered, and can be useful for surgeons in order to choose the adequate shunt, based on the required AH flow rate for a specific patient.

Practical implications: The present numerical approach, employing the generalized porous medium model, represents a useful tool to study the fluid dynamics of ocular drainage devices and to design these shunts, in order to reduce post-operative complications.

Originality/value: The generalised porous medium model is here applied for the first time to simulate the interaction of ocular drainage devices with the surrounding porous tissues of the eye.

Keywords: *Numerical modelling, Finite element method, Eye, Ocular Pathology, Patient specific, Surgery.*

Paper type: Research paper

NOMENCLATURE

D = diameter (m)

F = Forchheimer coefficient

h = local element size (m)

N = shape function

p = pressure (Pa)

t = time (s)

$\tilde{u}_i$ = intermediate velocity components (m/s)

u_k = mean velocity in the element (m/s)

u = velocity vector (m/s)

Greek symbols

β = artificial compressibility (m/s)

δ = Kronecker delta

Δt = time-step (s)

ε = porosity

κ = permeability

μ = dynamic viscosity ($\mathrm{Pa \cdot s}$)

ρ = density ($\mathrm{kg/m^3}$)

τ = deviatoric stress ($\mathrm{N/m^2}$)

Ω = element

Acronyms

AC = Anterior Chamber

AH = Aqueous Humor

ASCS = Anterior Suprachoroidal Space

CBS = Characteristic Based Split

GMS = Gold Micro Shunt

IOP = Intraocular Pressure

PSCS = Posterior Suprachoroidal Space

SCS = Suprachoroidal Space

SSD = Silicon Shunt Device

Subscripts

art = artificial

conv = convective

diff = diffusive

eff = effective

f = fluid

pr = pressure

*st*2 = second step

*st*3 = third step

Superscripts

n = iteration

1. INTRODUCTION

Glaucoma is the second leading cause of blindness in human eye. It is a disease of the optic nerve, which leads to optic disc excavation with death of a substantial number of retinal ganglion cells in the inner retina and loss of their axons in the optic nerve, with consequent vision loss and, in severe

cases, blindness. Data from population-based surveys indicate that one in 40 adults over forty years old has glaucoma with loss of visual function, corresponding to 60 million people worldwide being affected and more than 8 million being bilaterally blind [1]. In developed countries, an additional 50% of people are affected by glaucoma but are not aware of their disease, and in the developing countries the awareness is even lower [2]. Glaucoma is the second leading cause of vision loss in the world, and improved methods of screening and therapies for its treatment are urgently needed [2].

The primary reason of glaucoma (its main risk factor) is the abnormality of IntraOcular Pressure (IOP), the principal factor currently treatable. The adverse effects of raised IOP can be rectified by using various medical and surgical techniques, aimed at lowering IOP towards safe levels in individual patients, which can improve the eye vision to a certain extent. When this pressure is lowered by 20-40% with respect to its initial abnormal values, the average rate of progressive vision loss is halved [1].

Three main approaches can be followed in the treatment of glaucoma: (i) medical: hypotensive eye drops reduce the production of Aqueous Humor (AH) or increase its outflow; (ii) paramedical: Selective Laser Trabeculoplasty is able to induce a stretching of trabecular meshwork in patients not yet undergoing drug treatment; (iii) surgical: the principle of glaucoma surgery is to increase AH outflow from the eye, with consequent reduction of IOP [3].

Surgery is used for non-responsive cases to medical treatment and it is divided into two main sub-categories: (a) conventional treatments creating a link between the Anterior Chamber (AC) and the sub-conjunctival space of the eye, such as filtration procedures (trabeculectomy) or Molteno, Baerveldt, Krupin and Ahmed drainage valves [4-9]; (b) recent treatments creating a link between the AC and the Suprachoroidal Space (SCS), using devices such as the SOLX® Gold Micro Shunt (GMS) and the novel Silicon Shunt Device (SSD) studied in the present work [10-12].

This work is concerned with the second surgical sub-category, and aims at employing the generalized porous medium model to compare the fluid dynamics performance of the SOLX® GMS and of the novel SSD, proposed by some of the authors of this work in a recent clinical study [12]. Such a modeling study can support the surgeons to plan the surgical procedure and to choose the most effective ocular drainage device for their patients.

In a variable percentage of patients, filtration procedures and drainage valves (first surgical sub-category) lead to significant post-operative complications such as bleb leaks, hypotony, blebitis, endophthalmitis and bleb encapsulation, that indicate failure of IOP control [12-15]. As a consequence, research efforts are targeted to design safe bleb-less procedures, in order to maintain long-term surgical success of all available filtration based surgical procedures.

On the other hand, the second surgical sub-category discussed previously includes bleb-less surgical approaches [10-12], which exploit and enhance alternative AH outflow pathways. Among the devices used in these approaches, the SOLX® GMS is a biocompatible device made of gold flat plates containing microchannels, that create a connection between the AC and the Anterior SupraChoroidal (supraciliary) Space (ASCS), increasing the uveoscleral flow, as shown in clinical studies [11, 12]. The novel SSD, that has been recently employed by some of the authors in a pilot study [12], is a microtube made of silicon that connects the AC to the Posterior SupraChoroidal Space (PSCS). The operating principle of both shunts is based on the natural hydrostatic pressure difference between the AC and the SCS, that is the driving force of AH flow through the device. In practice, the AC pressure coincides with the IOP. The AH is evacuated from the AC through the device, and it flows through the SCS via the choroidal vascular system or by gradually flowing through the scleral layers and the conjunctiva, without the creation of blebs [12]. To the authors' knowledge, no experimental data are available in the literature on pressure gradients in human eyes, and measured values of pressure difference between AC and SCS have been presented for cynomolgus monkeys by Emi et al. [16]. On the basis of that study, at an IOP of 15 mmHg,

pressure in the ASCS was 0.8±0.2 mmHg smaller than IOP, while pressure in the PSCS was 3.7±0.4 mmHg smaller than IOP. The uveoscleral outflow of the AH throughout the SCS is commonly considered as pressure-independent, whereas the AH outflow throughout the trabecular meshwork increases almost linearly with the increase of IOP [17].

In terms of results obtained with the use of the SOLX® GMS, Melamed et al. [11] reported a 79% surgical success, defined as a post-operative IOP greater than 5 mmHg and less than 22 mmHg, with or without anti-glaucoma medications in the last follow-up, while Mastropasqua et al. [12] reported 57% successful implantations, defined as a reduction of the postoperative IOP of 66% with respect to the preoperative one, with or without anti-glaucoma treatment. Mastropasqua et al. explained different failure mechanisms of the GMS implantations: the formation of a fibrotic capsule around the device, that isolates it from the surrounding tissues, or a connective invasion/occlusion of the device channels and holes. Both mechanisms cause significant reduction of the AH outflow, with consequent malfunction of the implanted device, that does not allow the required amount of AH to reach and permeate the sclera.

On the other hand, preliminary results for installations of the novel SSD prove a higher success rate, obtaining a 90% of patients with post-operative IOP lower than 21 mmHg without any medication [12].

On the basis of the authors' knowledge, numerical studies comparing the fluid dynamics performance of different ocular drainage devices, by using the generalized porous medium model to analyse the interaction between the device and the surrounding tissues, are not present in the available literature. However, the need to have a clear understanding of the local phenomena that occur in the eye, also by means of a numerical modelling approach, is recognized in the scientific community [18, 19], such as the role of porous media in biological tissues [20]. Therefore, the authors employ for the first time the generalized porous medium model to study the fluid dynamics of the GMS and of the novel SSD and the surrounding porous tissues, by using the Characteristic

Based Split (CBS) scheme, already used for biomedical applications [21, 22] and validated against benchmark problems [23-26]. The objective of the work is to compare the performance of these devices in order to understand their fluid dynamic characteristics, so that any potential blockage or malfunction problem can be identified. The present work reports an estimation of the AH drainage through the two devices considered, and the results indicate a possible reason for the differences in the performance of these two devices.

The paper is organized as follows: the next section presents a description of the GMS and of the novel SSD; in section 3, the governing equations are reported. In section 4, the three-dimensional fully explicit CBS scheme is briefed, in terms of temporal and spatial discretizations. Section 5 shows the results obtained and some conclusions are drawn in the last section.

2. DESCRIPTION OF THE TWO SHUNTS

The SOLX® GMS is a non-valved flat-plate drainage device made of 24-K medical-grade (99.95%) gold [11]. The GMS width, length and thickness are 2.5 mm, 5.2 mm, and 44 μm, respectively. The geometrical characteristics of the shunt modelled in this work are presented in Figure 1. The AH enters the device from the side with rounded corners, positioned in the AC, and flows through the shunt driven by pressure difference between the AC and the ASCS. The inflow compartment is connected to the outflow compartment through microchannels, that allow the AH flow in the device orthogonally to the plates. The design of the GMS considered in the present work contains 9 microchannels located at the centre of the device [11]. The microchannels width and height are 24 μm and 50 μm, respectively. The inflow compartment of the GMS contains 60 holes of 100 μm in diameter and one 300 μm diameter hole on both plates of the device and 10 additional 50 μm lateral openings, that allow the inflow of AH. The outflow compartment contains a grid of 117 holes of 110 μm in diameter on both the plates of the shunt and 12 additional 50 μm openings, to allow the outflow of AH, as sketched in Figure 1.

Implantation of the GMS is typically performed under topical anaesthesia, sometimes augmented with subconjunctival lidocaine. The gold shunt can be inserted in any quadrant. It is important to select an area with healthy sclera and conjunctiva, to ensure a watertight closure and prevent bleb formation. Following the creation of a conjunctival peritomy, a 3-4 mm full thickness scleral incision is created 2–3 mm posterior to the limbus, to expose the supraciliary space. A scleral pocket at 95% depth is then fashioned, using a crescent knife to extend all of the way to the scleral spur. While the eye is still pressurized, the dissection is continued posteriorly into the suprachoroidal space. Subsequently, the anterior chamber is entered after the anterior chamber is stabilized with viscoelastic or by anterior chamber maintainer. The GMS is then delicately positioned with the proximal end in the anterior chamber and the distal end in the suprachoroidal space. Finally, the scleral incision is closed with multiple 10-0 nylon sutures and the conjunctiva is reapproximated with a 10–0 vicryl suture. Given the ab-externo approach with the conjunctival dissection, this procedure falls into the category of surgeries commonly referred to as blebless ab-externo glaucoma surgery.

The novel SSD adopted by some of the authors in a recent pilot study consists of a silicon micro tube with length, interior and exterior diameter of 8.0 mm, 320 μm and 640 μm, respectively [12]. In particular, a case series study of trabeculectomy versus SSD implant has been carried out on patients with open-angle glaucoma and morpho/functional worsening, despite maximal drug therapy [12]. The pilot study reported higher success rate in the patients with SSD implants at 12 months after surgery, in terms of less surgical complications and better post-operative IOP control. In particular, the implant has given excellent results in terms of significative IOP reduction, allowing at the same time to keep a physiological depth of anterior chamber and low grade of intraocular inflammation. One case of early hypotony was noticed, however no excessive drainage has been observed later [12].

The simple geometry of the novel SSD allows to obtain a regular AH flow inside the device, and is considered to be responsible for the excellent percentage (90%) of complete success of the installations of the shunt obtained in the randomized comparative study [12].

In the present work, the novel SSD is analysed numerically. In order to give a clear view of the actual installation of the device, a sketch of the anterior section of a human eye after installation of a drainage device is reported in Figure 2, while the surgical installation stages of the novel SSD are reproduced in Figure 3. The conjunctiva and Tenon's capsule were dissected from the superior limbus for approximately 4 clock hours to expose the sclera, and diathermy was applied to obtain a relatively dry field. A scleral incision at 4 mm from the limbus (1x4mm) was created with a crescent blade and the underlying choroid was exposed. A blunt spatula was inserted in the suprachoroidal space to create a real space until anterior chamber, creating a minimal cyclodialysis. All the surgeries were not combined. The authors take into account modifications to the above geometry employed in the experiments: changes in the diameter of the shunt and a variable number of radial holes for AH outflow control are considered in the present simulations, as shown in Figure 4.

3. THE MATHEMATICAL MODEL

The present mathematical model is based on the generalized approach for flow through porous media, that is very useful to study fluid dynamics problems where a free fluid and a porous medium are in contact. In this case, the porous medium is represented by ocular tissues, such as choroid and sclera, that are present in correspondence of the outflow section of the device implanted in the patient's eye, where the AH is drained. Therefore, the motion of the fluid inside the device is reproduced by solving free fluid flow equations, while the flow outside the device at the outlet section (interface between free fluid and porous medium) is reproduced by solving the porous medium flow equations.

The present problem has been solved by using a single-domain approach for the device and for the surrounding tissues at the outlet section, opportunely setting the properties of the medium for the free fluid domain and for the porous domain. This procedure for treating interface problems can be easily employed by using the generalized porous medium model [23, 24, 26]. In fact, this model is a flexible tool, since it reduces to the Navier-Stokes equations for porosity and permeability values equal to one and infinite, respectively, allowing to reproduce the internal fluid dynamics of the two shunts described in the previous section. Instead, if porosity and permeability assumes finite values, the AH outflow through the porous tissues surrounding the outlet section of the devices in the suprachoroidal space is simulated.

The AH is considered as a Newtonian incompressible fluid with density of 1000 kg/m^3 and dynamic viscosity of $7.5\cdot10^{-4}$ kg/(m·s) at 37°C [27].

The generalized model for the description of fluid flow through saturated porous media has been used to reproduce the AH flow inside the device and through the porous tissues. Assuming the porous medium to be fully saturated, under local thermal equilibrium, the generalized model for uniform properties of the porous medium, filled with a single phase incompressible fluid, can be written in indicial notation as:

Mass conservation equation

$$\frac{\partial u_i}{\partial x_i} = 0 \qquad (1)$$

Momentum conservation equation

$$\frac{\rho}{\varepsilon}\frac{\partial u_i}{\partial t} + \frac{\rho}{\varepsilon^2}u_j\frac{\partial u_i}{\partial x_j} = -\frac{\partial p_f}{\partial x_i} + \frac{\mu_{eff}}{\varepsilon}\frac{\partial \tau_{ij}}{\partial x_j} - \frac{\mu_f}{\kappa}u_i - \rho_f\frac{F}{\sqrt{\kappa}}|\mathbf{u}|u_i \qquad (2)$$

where the deviatoric stress is defined as:

$$\tau_{ij} = \frac{\partial u_i}{\partial x_j} + \frac{\partial u_j}{\partial x_i} \qquad (3)$$

The Navier-Stokes equations reproducing the fluid motion inside the devices can be obtained directly from the above generalized model equations by just setting $\varepsilon \to 1$ and $\kappa \to \infty$.

4. THE FULLY EXPLICIT CBS ALGORITHM

The Characteristic Based Split (CBS) algorithm used to solve numerically the generalized porous medium model reported in the previous section is based on the temporal discretization along characteristics, and spatial discretization obtained by employing the standard Galerkin finite element procedure [28, 29].

The stable fully explicit CBS scheme employed in the present work has been validated for different thermo-fluid dynamics problems [23-26], and has been successfully applied in the present paper to effectively solve fluid flow in ocular drainage devices employed for the treatment of glaucoma. The fundamental steps of the explicit CBS scheme are presented in the following. After the temporal discretization along the characteristics, these steps can be written as:

Step 1: Intermediate velocity calculation

$$\tilde{u}_i^{n+1} = u_i^n \left(1 - \Delta t \varepsilon P\right)^n - \Delta t^n \left[\frac{u_j}{\varepsilon} \frac{\partial u_i}{\partial x_j} - \frac{\mu_{eff}}{\varepsilon} \frac{\partial^2 u_i}{\partial x_i^2} - \frac{\Delta t}{2\varepsilon} u_k \frac{\partial}{\partial x_k} \left(u_j \frac{\partial u_i}{\partial x_j} \right) \right]^n \tag{4}$$

where $P = \left(\frac{\mu_f}{\kappa} + \rho_f \frac{F}{\sqrt{\kappa}} |\mathbf{u}| \right)$. The higher-order terms in the above equation appear from the discretization along the characteristics.

Step 2: Pressure calculation

$$p_{art}^{n+1} = p_{art}^n - \left(\beta^2 \Delta t\right)^n \frac{\rho_f}{\varepsilon} \frac{\partial \tilde{u}_i^{n+1}}{\partial x_i} + \left(\beta^2 \Delta t^2 \frac{\partial^2 p_{art}}{\partial x_i^2} \right)^n \tag{5}$$

Step 3: Velocity correction

$$u_i^{n+1} = \tilde{u}_i^{n+1} - \varepsilon \Delta t^n \left(\frac{\partial p_{art}}{\partial x_i} + \frac{\Delta t}{2} u_k \frac{\partial}{\partial x_k} \frac{\partial p_{art}}{\partial x_i} \right)^n \tag{6}$$

The superscripts *n+1* and *n* refer to the iterative procedure and not to actual time levels.

The three-dimensional spatial discretization of the above time discrete equations can be obtained through standard Galerkin finite element procedure and tetrahedral elements. Within an element, each variable is calculated through linear approximation on the basis of nodal values, according to the following equation:

$$\phi = \sum_{n=1}^{4} N_n \bar{\phi}_n \tag{7}$$

where N_n is the shape function at node n and $\bar{\phi}_n$ is the value of the generic variable ϕ at node n. The spatial approximation applied to the 3D explicit CBS steps leads to the following final matrix form of the three steps:

Step 1: Intermediate velocity calculation

$$\mathbf{M}\tilde{u}_i^{n+1} = \left(1-\Delta t\varepsilon P\right)^n \mathbf{M}u_i^n - \Delta t^n \left[\frac{1}{\varepsilon}\mathbf{C}u_i + \mu \mathbf{K}_d u_i + \frac{\Delta t}{2\varepsilon}\mathbf{K}_u u_i - \mu \mathbf{f}_d - \frac{\Delta t}{2\varepsilon}\mathbf{f}_u\right]^n \tag{8}$$

Step 2: Pressure calculation

$$\mathbf{M}p_{art}^{n+1} = \mathbf{M}p_{art}^n - \left(\beta^2\Delta t\right)^n \left[\frac{1}{\varepsilon}\mathbf{D}\tilde{u}_i^{n+1}\right] - \left(\beta^2\Delta t^2\right)^n \left[\mathbf{K}_{pr}p_{art} - \mathbf{f}_{pr}\right]^n \tag{9}$$

Step 3: Velocity correction

$$\mathbf{M}u_i^{n+1} = \mathbf{M}\tilde{u}_i^{n+1} - \Delta t^n \left[\varepsilon \mathbf{D}p_{art} - \varepsilon\frac{\Delta t}{2}\mathbf{K}_u p_{art}\right]^n \tag{10}$$

Where $\mathbf{M}$ is the mass matrix, $\mathbf{C}$ is the convection matrix, $\mathbf{K}_d$ is the diffusion matrix, $\mathbf{K}_u$ is the stabilization matrix obtained from higher-order terms, $\mathbf{f}_d$ and $\mathbf{f}_u$ are the boundary vectors from the momentum equation, $\mathbf{K}_{pr}$ is the stiffness matrix, $\mathbf{f}_{pr}$ is the boundary vector from the pressure equation, $\mathbf{D}$ is the gradient matrix. Details of all the terms presented in Equations (8)-(10) are given in references [28, 29]. The mass matrix is lumped using a standard row-summing approach, and the result is a fully matrix free procedure, particularly suitable to solve three-dimensional problems with a large number of grid elements.

5. COMPUTATIONAL DOMAINS AND BOUNDARY CONDITIONS

In this section, the computational domains and the boundary conditions employed for the two drainage devices are shown. For the pre-processing stage, the commercial software Comsol Multiphysics has been used. The first sub-section concerns the SOLX® GMS [11], while the second one concerns the novel SSD employed in a recent clinical study [12].

5.1. SOLX® Gold Micro Shunt (GMS)

The considered geometry is reported in Figure 1. The data have been taken from reference [11]. Since information on the exact position of holes and channels are not available, the geometry has been reproduced as shown in Figure 1, in order to obtain a fluid dynamic symmetry with respect to the vertical middle plane along AH flow direction. The computational domain, together with the boundary conditions employed, are sketched in Figure 5, while Figure 6a shows a detail of the unstructured computational grid employed near the microchannels. The mesh is composed of 2,369,419 tetrahedral elements.

The human tissues (sclera and choroid) have been reproduced as porous media with permeability of $2.5 \cdot 10^{-13}\ \mathrm{m}^2$; their thickness has been considered equal to 0.3 mm [28, 31]. The upper and lower surfaces of holes and the lateral openings in the inflow compartment are subject to the AC pressure. The surfaces of the porous tissues in correspondence of the outflow compartment are subject to the ASCS pressure. The AC pressure value considered in the simulations is 18.2 mmHg (2426 Pa), corresponding to the mean value measured by Melamed et al. within their clinical study [11]. The ASCS pressure value has been taken equal to 17.4 mmHg (2320 Pa), corresponding to a pressure difference between AC and ASCS of 0.8 mmHg, on the basis of the only experimental data available in the literature, reported by Emi et al. [16]. On the middle vertical plane in flow direction, fluid dynamic symmetry boundary conditions are imposed. Wall boundary conditions, corresponding to zero value of the three components of the velocity vector, are imposed on all other surfaces of the computational domain.

5.2. Novel Silicon Shunt Device (SSD)

The considered geometry is reported in Figure 4, while the computational domain, together with the boundary conditions employed, are sketched in Figure 7. Figure 6b shows a detail of the unstructured computational grid employed near the inflow section. The mesh is composed of 290,771 tetrahedral elements.

The same approach employed for the GMS to reproduce the human tissues has been used for the SSD. The inflow section of the microtube is subject to the AC pressure, while the surfaces of the porous tissues in correspondence of the outflow compartment are subject to the PSCS pressure. The AC pressure value considered in the simulations is 12 mmHg (1600 Pa), corresponding to the mean value measured by some of the present authors in a pilot study on patients after surgical insertion of the microtube [12]. The PSCS pressure value has been taken equal to 8.3 mmHg (1107 Pa), corresponding to a pressure difference between AC and PSCS of 3.7 mmHg, on the basis of the only experimental data on pressure difference available in the literature [16]. Wall boundary conditions, corresponding to zero value of the three components of the velocity vector, are imposed on all other surfaces of the computational domain.

This device, with very simple geometry, has given encouraging results in the recent pilot study conducted [12]. The configuration of the SSD employed in the clinical study had no radial holes, and it was a simple microtube of the same length and exterior diameter of the one studied here, with an interior diameter fixed to 320 μm. After the surgery, the microtube assumes a slight deformed shape, but the entity of this deformation is not expected to modify the present considerations. In this work, the presence of radial holes and the effect of changing the SSD diameter are analysed.

6. RESULTS AND DISCUSSION

In this section, the numerical results obtained for AH flow driven by pressure difference in the SOLX® GMS [11] and in the novel SSD employed in a recent pilot study [12] are presented here for the first time.

6.1. SOLX® Gold Micro Shunt (GMS)

The velocity field of the AH inside the device, driven by the pressure difference between AC and ASCS, is shown in Figure 8. From the analysis of the figure, it is evident that the velocity of AH at the microchannels is high compared to the inlet and outlet section. The device studied in the present work is able to obtain an AH drainage of $1.04\ \mu l/min$, that is significantly smaller than normal AH production values for men and women, estimated at $2.2-3.1\ \mu l/min$ [32, 33]. Once the AH enters the shunt from the 61 holes present on both the parallel plates and from the 10 lateral openings, it accelerates in correspondence of the microchannels in order to flow towards the outflow compartment. Figure 9 shows the velocity profiles at two sections of the GMS: one in correspondence of the holes' line just before the entrance of the microchannels, and another in correspondence of the entrance of the microchannels. From the analysis of the figure, it is evident that the AH velocity increases of one order of magnitude in a very small space along the flow direction (less than 0.2 mm). In fact, the internal fluid dynamics of the GMS is characterized by evident velocity gradients of several orders of magnitude between different areas of the shunt. In the regions near the inlet and outlet sections, the velocity values are found out to be smaller than 10^{-5} mm/s, and AH flow is practically absent, as shown in Figure 10. In this figure, the non-coloured zones are those where velocity is larger than 10^{-5} mm/s. Since the AH does not move in an extended volume of the device, and the inflow and outflow through many holes is practically absent, the surrounding vessels in the AC and in the ASCS can easily penetrate the shunt through these holes, with consequent possible problems of blockage and malfunction of the GMS. Another problem could be related to the fluid accumulated on the walls next to the microchannels, where the AH is

stagnant, since an excessive amount of accumulated fluid could cause their partial obstruction, limiting the drainage capacity of the device. Furthermore, the pressure difference existing between the AC and the ASCS is small (0.8 mmHg) and, as a consequence, the fluid motion inside the device is weak. If the outflow was targeted towards Posterior Suprachoroidal Space (PSCS), the higher pressure gradient would have led to an increased outflow. The choice to use the GMS to connect the AC to the ASCS, instead of the PSCS, which is characterized by a larger pressure difference (3.7 mmHg), could be probably due to avoid hypotonic conditions. If the device was designed and chosen on the basis of patient needs, such as preoperative IOP values and other preoperative medical considerations (depth or inflammation of anterior chamber), surgeons could employ a shunt more adaptable to a specific patient, reducing failures. However, these critical conditions have not been encountered in patients with surgical insertion of the novel SSD within the recent pilot study [12].

6.2. Novel Silicon Shunt Device (SSD)

When the simple microtube is employed, a parabolic fluid flow is obtained in the shunt after a short entrance length. The maximum value of velocity approaches 1.7 mm/s, significantly larger than the velocity values for the GMS, therefore AH accumulation is not expected to occur. Furthermore, the regular cylindrical geometry is another favourable factor to avoid fluid accumulation. A volumetric flow rate (drainage from the AC to the PSCS) of 2.57 μl/min is obtained, therefore significantly higher than the value corresponding to GMS and comparable to normal human values. If this value is considered too large by surgeons for patient needs, such as preoperative IOP values and other preoperative medical considerations (depth or inflammation of anterior chamber), a SSD with smaller diameter can be employed. In fact, a drainage of 1.92 μl/min and of 1.52 μl/min is obtained by reducing the diameter of the microtube to 280 μm and to 250 μm, respectively, as reported in Table 1.

The surgeons' concern, other than obtaining a lower postoperative IOP, is to keep an adequate anatomical morphology. The SCS is connected with the AC, therefore if the flow resistance was reduced (in order to obtain a higher outflow) a significative depth reduction of the AC could be caused, with several anatomical damage (as corneal endothelial cell loss, intraocular inflammation etc.). However, these effects have not been observed in any patient of the pilot study described in section 2 employing the SSD [12]. For this reason, the authors consider the maximum diameter of 320 μm, corresponding to the one employed in the pilot clinical study.

Therefore, surgeons can choose implants with smaller diameter in patients with a depth of the anterior chamber smaller than 2 mm or in patients with an increased risk of contact between shunt and corneal endothelium. When the risk of contact between endothelium and shunt increases, the choice of a less bulky shunt exposes the patient to less risk of corneal decompensation. For example, in hyperopic patients the axial length and the depth of the anterior chamber are lower than in normal eyes. In the case of high hyperopia, these values are even more reduced. Therefore, these patients would be better candidates for smaller shunts.

Among the modifications to the SSD, 100 μm diameter radial holes have been considered on the lateral surface of the microtube, to control the AH flow rate through the device. These holes are subject to the pressure of the PSCS. The results in terms of AH volumetric flow rate (drainage) through the SSD with different interior diameters and number of radial holes are reported in Table 1. Surgeons could use this table to choose a device that better fit the patient specific needs. The use of radial holes is useful to manage the AH outflow with more flexibility with respect to the cases of simple microtubes. The devices employing three or six holes could be appropriate for patient needs, given the calculated values of AH outflow reported in Table 1, that are comparable to normal human values [32, 33]. On the other hand, Table 1 shows that the drainage calculated in presence of twelve holes is significantly larger than normal values for men and women.

This simple shunt can be a useful tool to be employed to control IOP, reducing post-operative complications due to accumulation of AH inside the device, thanks to its regular geometry. It also

enables surgeons to choose the device on the basis of patient specific needs (i.e. preoperative IOP values, depth or inflammation of anterior chamber), by using microtubes with different diameters and a variable number of radial holes. These considerations are supported by clinical results obtained within the pilot study described in section 2 [12].

7. CONCLUSIONS

In this paper, the generalized porous medium model has been employed to simulate the fluid dynamics in two ocular drainage devices, the SOLX® Gold Micro Shunt (GMS) and the novel microtubular Silicon Shunt Device (SSD), taking into account the presence of the surrounding porous tissues of the eye. The main outcomes of the present work are:

- The Aqueous Humor (AH) flow in the GMS encounters stagnation areas and low velocity regions, with consequent possible blockage and malfunction of the device;
- The novel SSD proposed by the authors allows to obtain an AH drainage comparable to normal human values, thanks to its regular microtubular geometry;
- The AH volumetric flow rate (drainage) has been calculated for different configurations of the SSD, by changing the diameter and/or employing a variable number of radial holes, in order to allow surgeons to choose the value that best fits patient specific needs, and to implant the most adequate shunt.

The authors believe that the present numerical simulation approach, based on the generalized porous medium model, represents a useful tool to study the fluid dynamics of ocular drainage devices and to design these shunts, reducing post-operative complications.

ACKNOWLEDGMENTS

Alessandro Mauro and Mario R. Romano gratefully acknowledge the financial support of TeVR SIR project n. RBSI149484, CUP E62I15000760008.

REFERENCES

1. Quigley, H.A. (2011), "Glaucoma. Seminar", The Lancet, Vol. 377, pp. 1367-1377.
2. Quigley, H.A. (1996), "Number of people with glaucoma worldwide", British Journal of Ophthalmology, Vol. 80, pp. 389-393.
3. Franzco, W.H.M., Yu, D.-Y. (2012), "Surgical management of glaucoma: a review", Clinical and Experimental Ophthalmology, Vol. 40, pp. 388-399.
4. Jones, E., Clarke, J., Khaw, P.T. (2005), "Recent advances in trabeculectomy technique", Current Opinion in Ophthalmology, Vol. 16, pp. 107-13.
5. Hodkin, M.J., Goldblatt, W.S., Burgoyne, C.F., Ball, S.F., Insler, M.S. (1995), "Early clinical experience with the Baerveldt implant in complicated glaucomas", American Journal of Ophthalmology, Vol. 120, pp. 32-40.
6. Mermoud, A., Salmon, J.F., Alexander, P., Straker, C., Murray A.D. (1993), "Molteno tube implantation for neovascular glaucoma. Long-term results and factors influencing the outcome", Ophthalmology, Vol. 100, pp. 897-902.
7. Huang, M.C., Netland, P.A., Coleman, A.L., Siegner, S.W., Moster, M.R., Hill, R.A. (1999), "Intermediate-term clinical Experience with the Ahmed glaucoma valve implant", American Journal of Ophthalmology, Vol. 127, pp. 27-33.
8. Patel, S., Pasquale, L.R. (2010), "Glaucoma drainage devices: a review of the past, present, and future. Review", Seminars in Ophthalmology, Vol 25, pp. 265-70.
9. Coleman, A.L., Hill, R., Wilson, M.R., Choplin, N., Kotas-Neumann, R., Tam, M., Bacharach, J., Panek, W.C. (1995), "Initial clinical experience with the Ahmed glaucoma valve implant", American Journal of Ophthalmology, Vol. 120, pp. 23-31.
10. Minckler, D.S., Hill, R.A. (2009), "Use of novel devices for control of intraocular pressure. Review", Experimental Eye Research, Vol. 88, pp. 792-798.

11. Melamed, S., Simon, G.J.B., Goldenfeld, M., Simon, G. (2009), "Efficacy and Safety of Gold Micro Shunt Implantation to the Supraciliary Space in Patients With Glaucoma. A Pilot Study", Archives of Ophthalmology, Vol. 127, pp. 264-269.

12. Mastropasqua, L., Agnifili, L., Ciancaglini, M., Nubile, M., Carpineto, P., Fasanella, V., Figus, M., Lazzeri, S., Nardi, M. (2010), "In vivo analysis of conjunctiva in gold micro shunt implantation for glaucoma", British Journal of Ophthalmology, Vol. 94, pp. 1592-1596.

13. Romano, V., Romano, F., Mauro, A., Vinciguerra, R., Rinaldi, L., Angi, M., Romano, M.R., Costagliola, C. (2016), "Glaucoma Surgery: potential of a new uveoscleral outflow shunt", under review, International Ophthalmology.

14. Kee, C. (2001), "Prevention of early postoperative hypotony by partial ligation of silicone tube in Ahmed glaucoma valve implantation", Journal of Glaucoma, Vol. 110, pp. 466-469.

15. Feldman, R.M., Tabet, R.R. (2008), "Needle revision of filtering blebs", Journal of Glaucoma, Vol. 17, pp. 594-600.

16. Emi, K., Pederson, J.E., Toris, C.B. (1989), "Hydrostatic Pressure of the Suprachoroidal Space", Investigative Ophthalmology & Visual Science, Vol. 30, pp. 233-238.

17. Alm, A., Nilsson, S.F.E. (2009), "Uveoscleral outflow - A review", Experimental Eye Research, Vol. 88, pp. 760-768.

18. Avtar, R., Srivastava, R. (2006), "Modelling the flow of aqueous humor in anterior chamber of the eye", Applied Mathematics and Computation, Vol. 181, pp. 1336-1348.

19. Shafahi, M., Vafai, K. (2011), "Human eye response to thermal disturbances", Journal of Heat Transfer , Vol. 133, pp. 110091-110097.

20. Khaled, A.-R.A., Vafai, K. (2003) "The role of porous media in modeling flow and heat transfer in biological tissues", International Journal of Heat and Mass Transfer, Vol. 46, pp. 4989-5003.

21. Nithiarasu, P., Liu, C-B, Massarotti, N. (2007), "Laminar and turbulent flow calculations through a model human upper airway using unstructured meshes", Communications in Numerical Methods in Engineering, Vol. 23, pp. 1057-1069.

22. Nithiarasu, P., Hassan, O., Morgan, K., Weatherill, N.P., Fielder, C., Whittet, H., Ebden, P., Lewis, K.R. (2008), "Steady flow through a realistic human upper airway geometry", International Journal for Numerical Methods in Fluids, Vol. 57, pp. 631-651.

23. Massarotti, N., Ciccolella, M., Cortellessa, G., Mauro, A (2016), "New benchmark solutions for transient natural convection in partially porous annuli", International Journal of Numerical Methods for Heat & Fluid Flow, Vol. 26, pp. 1187-1225.

24. Arpino, F., Carotenuto, A., Massarotti, N., Mauro, A. (2013), "New solutions for axial flow convection in porous and partly porous cylindrical domains", International Journal of Heat and Mass Transfer, Vol. 57, pp. 155-170.

25. Arpino, F., Cortellessa, G., Dell'Isola, M., Massarotti, N., Mauro, A. (2014), "High Order Explicit Solutions For Transient Natural Convection of Incompressible Fluids in Tall Cavities", Numerical Heat Transfer, Part A: Applications, Vol. 66, pp. 839-862.

26. Arpino, F., Cortellessa, G., Mauro, A. (2015), "Transient thermal analysis of natural convection in porous and partially porous cavities", Numerical Heat Transfer; Part A: Applications, Vol. 67, pp. 605-631.

27. Heys, J.J., Barocas, V.H., Taravella, M.J. (2001), "Modeling Passive Mechanical Interaction Between Aqueous Humor and Iris", Journal of Biomechanical Engineering, Vol. 123, pp. 540-547.

28. Zienkiewicz, O.C., Taylor, R.L., Nithiarasu, P. (2014), "The Finite Element Method for Fluid Dynamics", seventh ed., Elsevier, Oxford.

29. Nithiarasu, P., Lewis, R.W., Seetharamu, K.N. (2016), "Fundamentals of the finite element method for heat and mass transfer", second ed., John Wiley & Sons, Chichester.

30. Lee, S.B., Geroskia, D.H., Prausnitzb, M.R., Edelhauser, H.F. (2004) "Drug delivery through the sclera: effects of thickness, hydration, and sustained release systems", Experimental Eye Research, Vol. 78, pp. 599-607.

31. Miyake, M., Tsujikawa, A., Yamashiro, K., Ooto, S., Oishi, A., Tamura, H., Nakata, I., Matsuda, F., Yoshimura, N. (2014), "Choroidal Neovascularization in Eyes With Choroidal Vascular Hyperpermeability", IOVS, Vol. 55, pp. 3223-3229.

32. McLaren, J.W. (2010), "Control of Aqueous Humor Flow", in Dartt, D.A., Besharse, J.C., Dana, R. (Eds.), Encyclopedia of the Eye, Elsevier, Oxford.

33. McLaren, J.W. (2009), "Measurement of aqueous humor flow", Experimental Eye Research, Vol. 88, pp. 641-647.

Table 1. AH volumetric flow rate (drainage) through the novel SSD (µl/min) obtained varying the diameter of the microtube and the number of 100 µm diameter radial holes.

D (µm) / n. holes	320	280	250
0	2.57	1.92	1.52
3	3.28	2.68	2.27
6	4.01	3.40	2.99
12	5.48	4.85	4.40

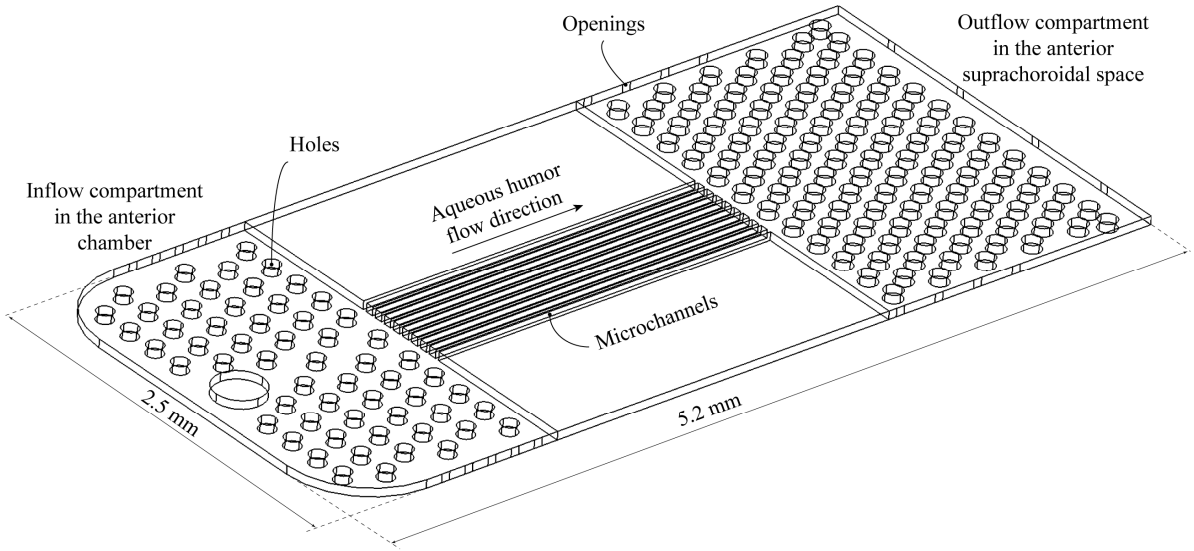

Figure 1. Schematic geometry of the SOLX® GMS [11].

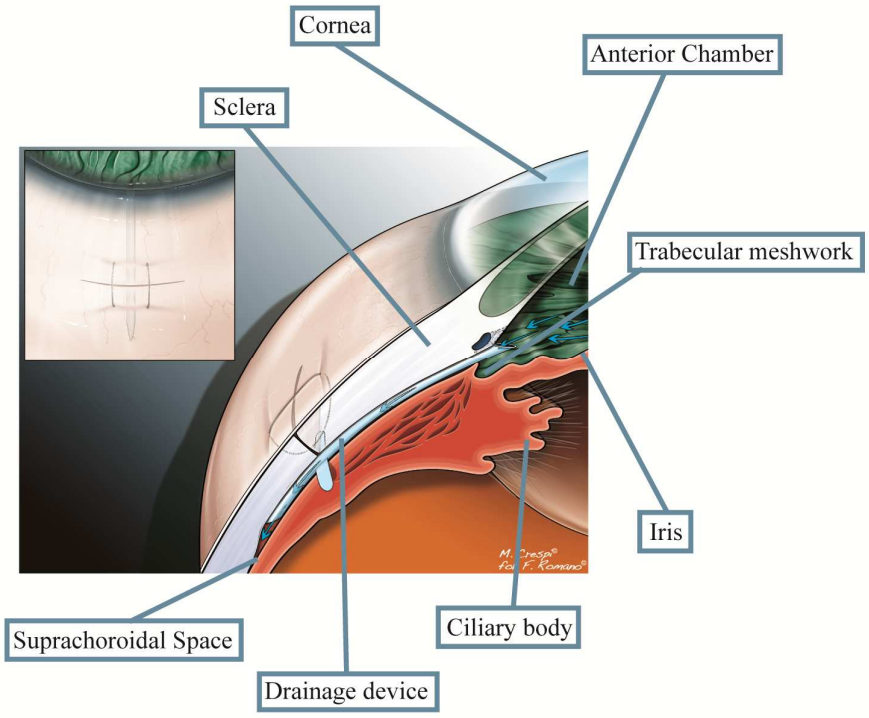

Figure 2. Sketch of the anterior section of a human eye after installation of a drainage device, with the description of the different parts.

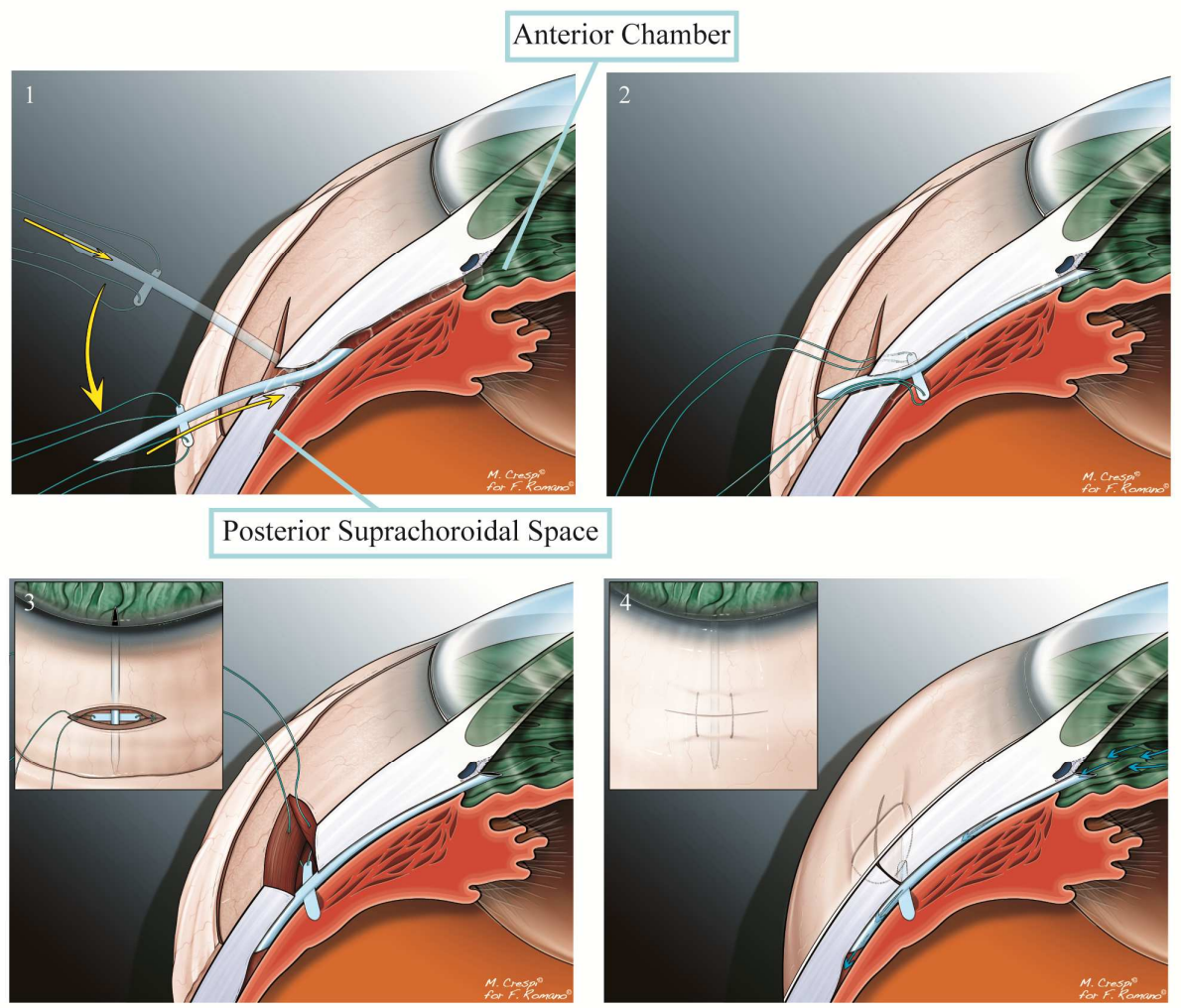

Figure 3. Surgical installation stages of the novel SSD: stage 1 (top left), stage 2 (top right), stage 3 (bottom left) and stage 4 (bottom right).

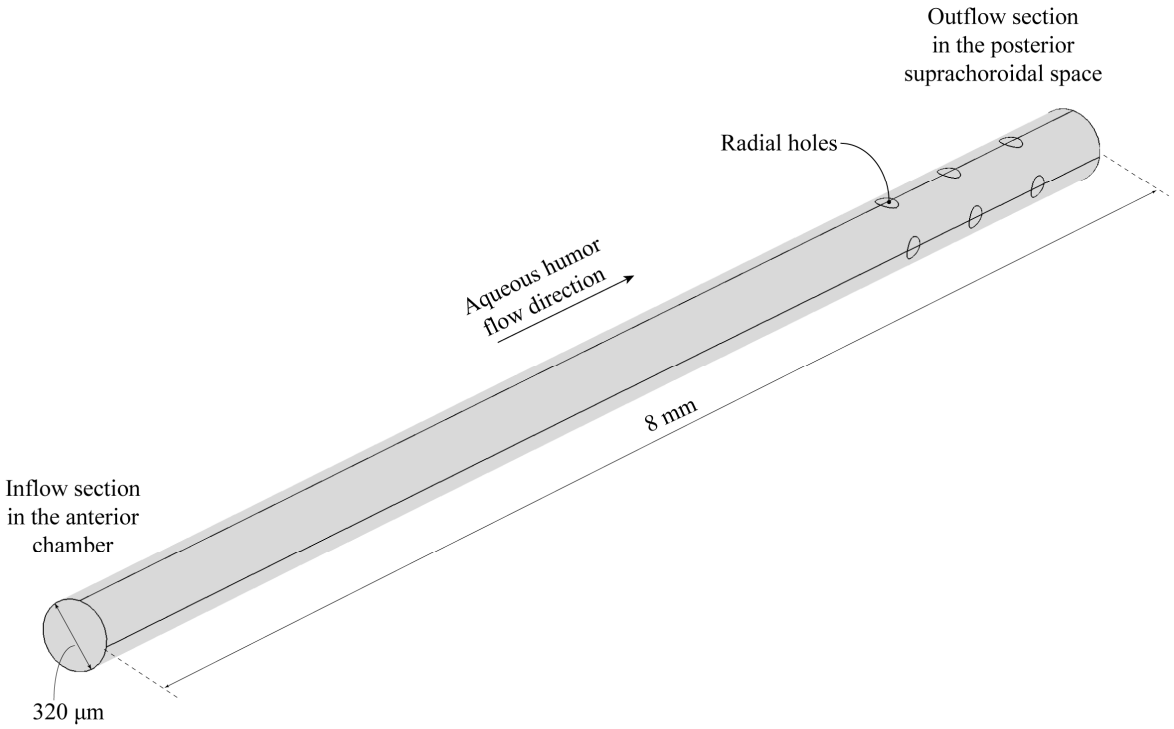

Figure 4. Schematic geometry of the novel SSD employed by the authors and its modifications (radial holes).

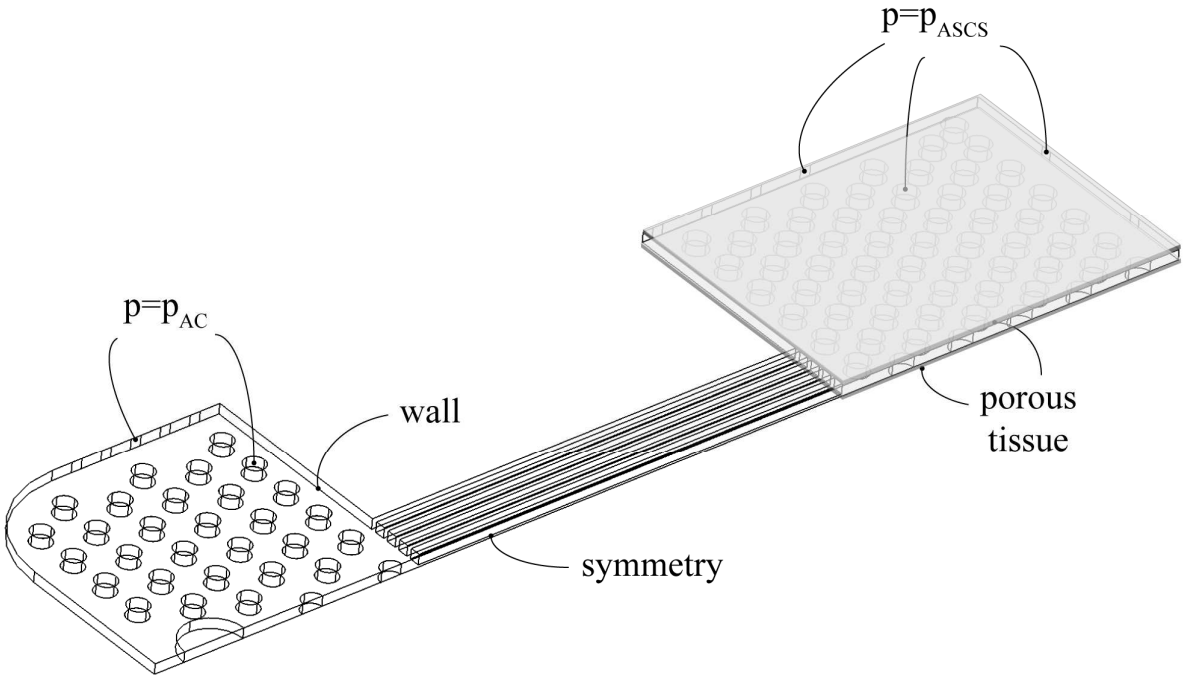

Figure 5. Computational domain and boundary conditions employed for the GMS.

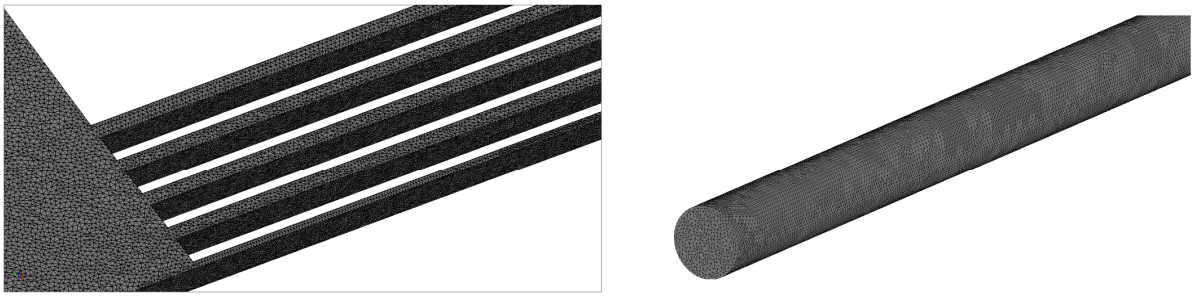

a b

Figure 6. Detail of the computational grid employed for: (a) the GMS near the microchannels (2,369,419 tetrahedral elements) and (b) the novel SSD near the inflow section (290,771 tetrahedral elements).

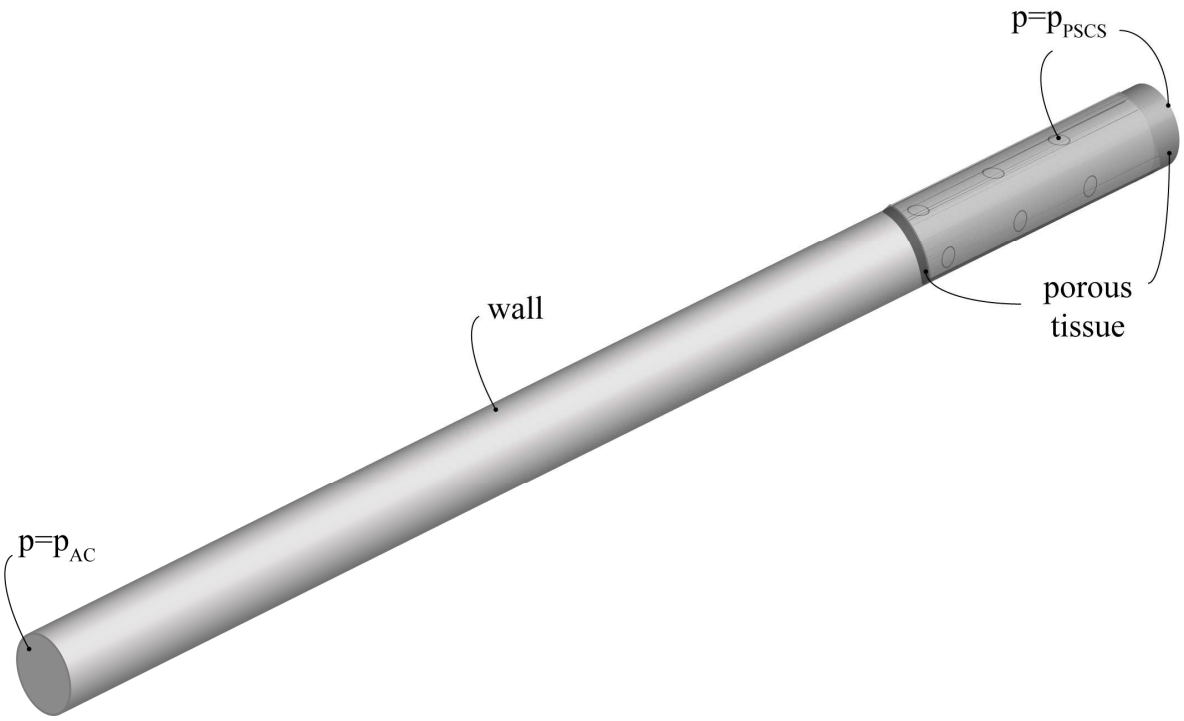

Figure 7. Computational domain and boundary conditions employed for the novel SSD.

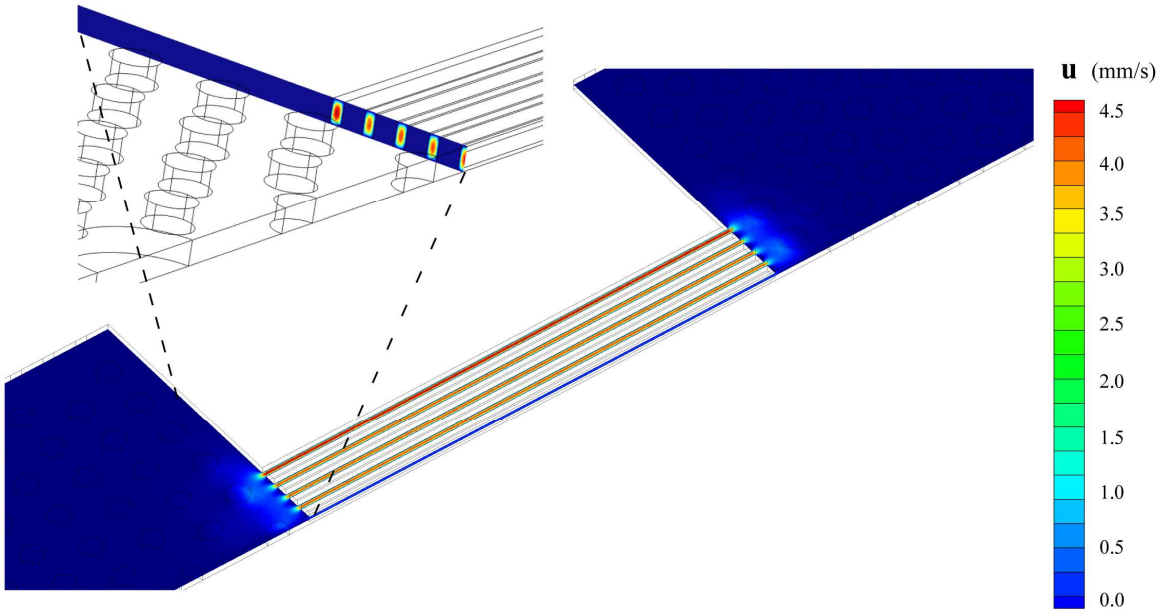

Figure 8. Velocity field in the GMS: detail in correspondence of the microchannels and zoom on the entrance of the microchannels.

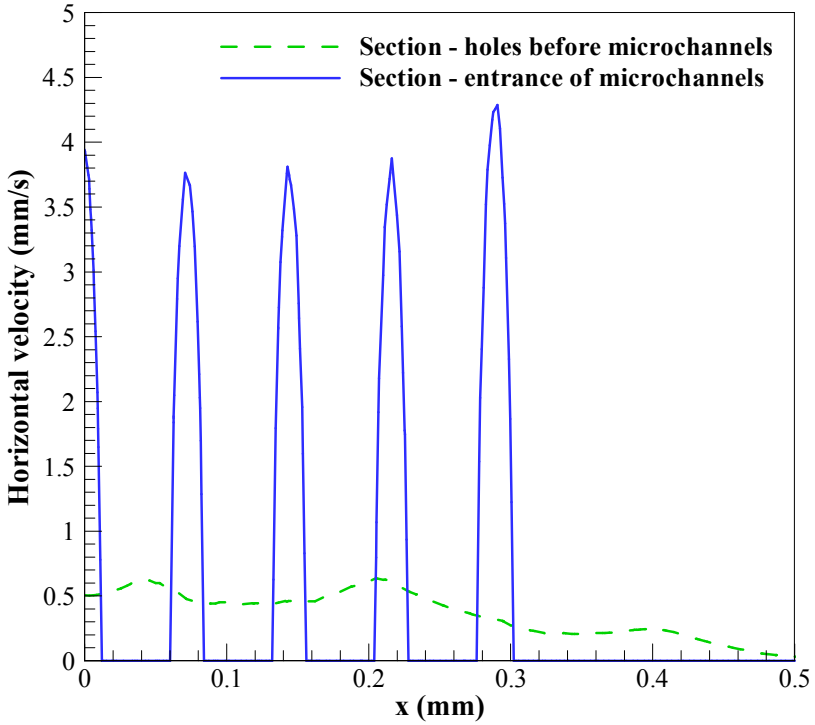

Figure 9. Velocity profiles at two sections of the GMS: in correspondence of the holes' line before the microchannels; in correspondence of the entrance of the microchannels.

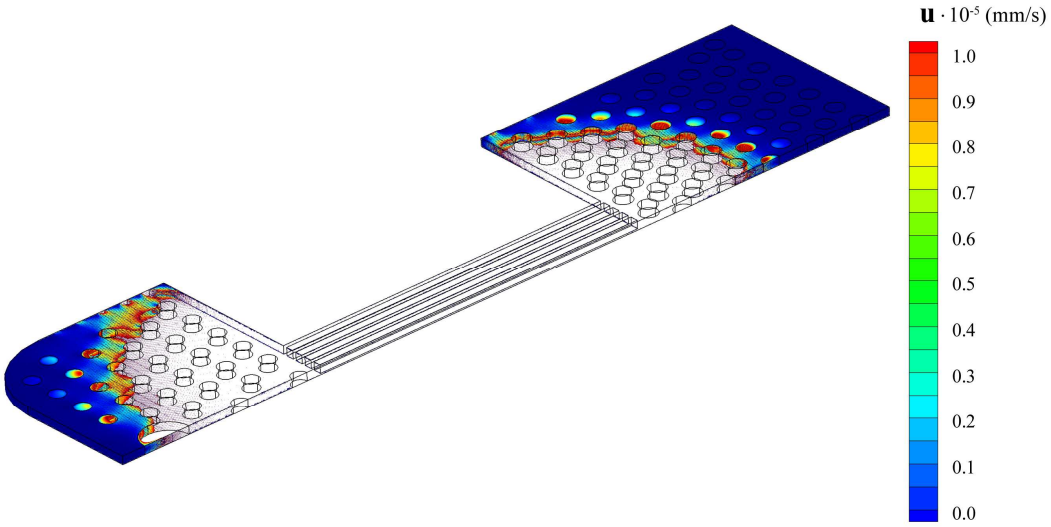

Figure 10. Velocity field in the GMS: stagnation zones (blue colour).